Computational Mechanics 25 (2000) 501–513 © Springer-Verlag 2000

An accurate boundary-element method for Stokes flow in partially covered cavities*

C. H. Driesen, J. G. M. Kuerten

Abstract The two-dimensional flow of a viscous fluid over an etched hole is computed with a boundary-element method. The etch-hole geometry contains sharp corners at which the solution of the traction boundary-integral equation is singular. Therefore, only the regular part of the solution is computed with the boundary-element method, using a singularity-subtraction method, and the singular part of the solution is added. However, there are regions in which these regular and singular parts are of almost equal magnitude, but different in sign. To avoid the subtraction and addition of large quantities where quantities of smaller order are computed a domain-decomposition technique is introduced. We show that the accuracy indeed increases by the described techniques. After extrapolation the results for a rectangular geometry agree very well with results obtained earlier with a semi-analytical method. A new integral formulation is derived for the stream function in the form of a boundary integral over the velocity and shear-stress components. Finally we show some results for arbitrary etch holes.

1 Introduction

The mathematical modelling of fluid flow in combination with mass or heat transport in cavities has been a topic of active research for the last three decades. Several articles have been written for a wide range of applications varying from the evolution of corrosion pits, heat transfer along rough surfaces, crystal-growth processes, electro-deposition, and mass transfer from cavities in artery walls. In most of the literature the computation of the fluid flow is combined with a computation of heat or mass transfer from the cavity to the surrounding fluid or, alternatively, from the fluid to the cavity walls.

In wet-chemical etching an almost similar problem arises, namely that of the fluid flow in a partially covered cavity as depicted in Fig. 1. Wet-chemical etching is an important technique in modern technology as can be exemplified by the production of oil filters, shadow masks for color TV sets, lasers and integrated circuits. An etching process of this kind can be described in the following way: A thin piece of metal is covered with a mask. A chemical solution is sprayed onto it, dissolving the metal which is not covered. Using this method we are able to make very detailed small products in an easy way. Because dissolution will occur in all directions, geometries such as that depicted in Fig. 1 will arise. Sideways etching under the masks is called the 'undercut' effect. The result of this effect is that the etch hole is larger, and the size of the etched product is smaller than the original mask pattern. These differences between products and masks can become very large, especially when we think of products with sizes which are of the same order as the thickness of the material. Therefore, research is necessary to obtain information about this effect in etching processes.

One of the subproblems in a numerical etching simulation is the computation of the fluid flow. The diffusion coefficient of the dissolution of metal in a wet-chemical etching process is very small (order $10^{-10}\,\mathrm{m^2\,s^{-1}}$). Therefore the etching simulation can be performed in a quasi-stationary way. Since the boundary of the etch hole moves very slowly in comparison with the fluid flow, we can compute the flow in each time step as if the boundary were stationary. As a possible application of wet-chemical etching, we can think of the etching procedure of small grooves in rotating disks, such as depicted in Fig. 2. These disks are used as electrodes. When the width W of the groove is small in comparison to the distance to the center of the disk, a two-dimensional approximation can be made as shown in Fig. 1. The fluid flow in this application is described by the incompressible Navier–Stokes equations. These equations are scaled by the model parameters and the inertial terms are neglected on account of the Reynolds number being small, thus resulting in the Stokes equations. However, since the diffusion coefficient is much smaller than the kinematic viscosity, the etching process is still convection-dominated. In the case of a uniform flow

Received 15 September 1999

*The work presented in this paper was carried out at the University of Twente, The Netherlands.

C. H. Driesen (✉)
KPN Research, P.O. Box 421, 2260 AK Leidschendam,
The Netherlands
e-mail: c.h.driesen@kpn.com

J. G. M. Kuerten
Department of Mechanical Engineering,
Eindhoven University of Technology,
P.O. Box 513, 5600 MB Eindhoven,
The Netherlands
e-mail: j.g.m.kuerten@wtb.tue.nl

This work was supported by STW, the Netherlands Technology Foundation, under project TWI44.3286. The authors wish to thank Prof. P.J. Zandbergen, Dr. H.K. Kuiken and Dr. D. Dijkstra for stimulating discussions and recommendations.

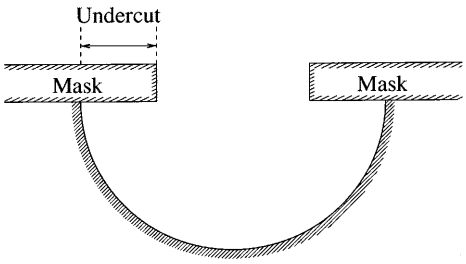

Fig. 1. Etch hole with undercut

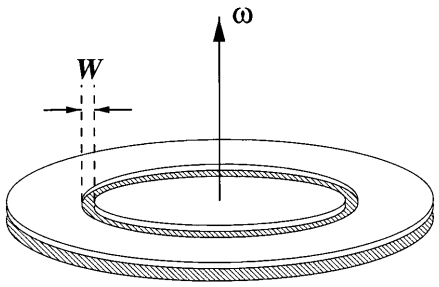

Fig. 2. Etching a groove in a rotating disk

along a cavity a vortex will arise in the interior. Due to the convection-dominated character of the process, transport of the 'polluted' solution takes place in a thin boundary layer along the rim of the vortex Kuiken [17]. The exchange of etching products occurs by means of diffusion across the streamline that separates the vortex from the outer flow.

In the simulations of Shin and Economou [24, 25] the velocity components and the concentration in an etch-hole geometry are computed by means of a finite-element method. However, since mass transport occurs only near the boundary and the dividing streamlines, it is more efficient to use methods which need only information from the boundary. These methods have the advantage that a computational grid for the interior is not required. In Kuiken [17] it is described how to compute the concentration in an etch hole without overhanging masks from the velocity and shear-stress components. The shear-stress components are needed at the boundary of the cavity, and the velocity components are needed at the separating streamline. These quantities required for the computation of the concentration can be computed with the boundary-element method which is presented in this paper.

The boundary-element method was first applied in linear elastostatics and potential problems and later also to two-dimensional Stokes flow and the associated biharmonic equation for the stream function. Bézine and Bonneau [1] were among the first to use the boundary-element method for the computation of Stokes flow in rather standard geometries. In Higdon [11] and Bohou [2] the method is applied to flow over rectangular holes.

When the geometry includes sharp corners, singularities arise near those corners. This problem was first encountered by Moffatt [20], who derived an expression for the singular behavior. This behavior can be included in the integral equations, to regularize the integrals near the corners. This singularity-subtraction method was used in Bohou [2], Hansen and Kelmanson [10] and

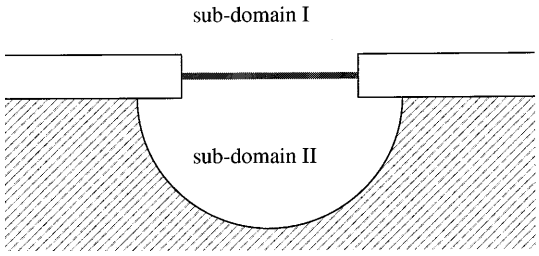

Fig. 3. Definition of sub-domains for the etch-hole geometry

Kelmanson [16] to increase the accuracy of the computations.

We have applied a boundary-integral equation method of the second kind as described in Ingber and Mondy [14] and Chien, Rajiyah and Atluri [3] to different etch-hole geometries. These geometries include sharp corners. We apply the singularity-subtraction technique as described in [20, 2, 10, 16] to regularize the integrals near these corners.

The singularity subtraction in our application has a disadvantage. The velocity near the bottom of the etch hole is the sum of two contributions, the regular part and singular part, which are of almost equal magnitude but different sign. Hence, small relative errors in the two contributions may result in large relative errors. One method to avoid this loss of accuracy is to use domain decomposition. In this paper we introduce two sub-domains as shown in Fig. 3 to improve the accuracy of the integrals. We believe that it is the first time that a domain-decomposition method is used in a boundary-element method applied to the Stokes equation. In De Haas [4], Hsiao and Wendland [13] and Greenbaum and Greengard [9] domain decomposition was already applied to a potential problem. In general, in a domain-decomposition method for boundary-element methods, a new boundary arises by splitting the domain. At this new boundary, all quantities are unknown. The solution is then obtained by an iterative process. In this paper, we first choose initial values for the velocity components. We compute an approximation for the shear-stress components with the equations for the first sub-domain. These stress components are used in the second sub-domain to compute a new approximation for the velocity components, and so on. The construction of a sequence of boundary conditions which is used here is also known as the Neumann–Dirichlet preconditioner [4], Funaro, Quarteroni and Zanolli [8, 9] and Hribersek and Skerget [12]. One advantage of domain decomposition in this application of the boundary-element method is that the results are more accurate, which is shown in Sect. 3. Another advantage is that CPU-time is saved when this method is used in a numerical simulation of wet-chemical etching. In such a simulation the flow needs to be computed in each time step for a geometry in which the etch-hole grows. However, the geometry of the first sub-domain of Fig. 3 remains the same. When we apply domain decomposition, it is not necessary to recompute the matrix for the unknown quantities of this sub-domain, which saves much CPU-time.

Using the boundary-element method with domain decomposition and a special treatment of the singularities we obtain accurate results for velocity and shear-stress

components. The accuracy is validated by grid refinement and a comparison with the results of Driesen [6]. In [6] the first accurate solutions of the biharmonic equation were computed for rectangular approximations of etch-hole geometries. The authors used a technique involving the matching of biorthogonal infinite eigenfunction expansions in different parts of the domain. Truncated versions of these series were used to compute a finite number of unknown coefficients. In this way the stream function and its derivatives were determined accurately in an arbitrary point. The validation shows an excellent agreement between semi-analytical and boundary-element results.

In order to apply the boundary-element method for a computation of concentration of dissolved material in a semi-analytical way following [17], it is necessary to know the positions of the free streamlines between the vortices inside of the etch-hole geometry. To obtain these positions, different methods can be used. For example, it is possible to compute velocities in a number of points, and obtain the position of the dividing streamlines by numerical integration. However, it is faster and more accurate to compute the stream function directly as a boundary integral. Therefore, a new integral formulation is derived. With this new formulation the stream function can be computed as a boundary integral over the shear-stress and velocity components.

Summarizing, the purpose of this paper is to provide an accurate solution method for the stream function and the velocity and shear-stress components in etch-hole geometries. These quantities are needed for a numerical simulation of wet-chemical etching, which will be the subject of future research.

In the next section, we give the mathematical formulation of the fluid-flow problem and we describe the integral equations for the unknown quantities. The singularity-subtraction method is described, as well as the domain decomposition. In Sect. 3 the implementation of the numerical integrations is described. We consider the accuracy of the computations by comparing them to the results derived in [6]. We show that the combination of singularity subtraction and domain decomposition leads to improved results, which are very accurate. Finally, in Sect. 4 we show some results for different geometries, which give insight in the character of the fluid flow inside holes of different shape.

2
Mathematical formulation

In this section we describe the integral equations used in this paper. We give the problem definition, the definitions of the standard integral equations and we derive the boundary-integral expression for the stream function. We describe the singularity-subtraction technique to remove the singularities at the sharp corners. Finally, in the last part of this section the domain decomposition is presented.

2.1
Problem definition

The fluid flow in this application is described by the Stokes equations

$$\nabla \cdot \boldsymbol{\sigma} = 0 \ , \tag{2.1}$$

and the continuity equation

$$\nabla \cdot \mathbf{u} = 0 \ . \tag{2.2}$$

The stress tensor $\boldsymbol{\sigma}$ is defined in the standard form:

$$\sigma_{ij} = -p\delta_{ij} + \left(\frac{\partial u_i}{\partial x_j} + \frac{\partial u_j}{\partial x_i}\right) \ , \tag{2.3}$$

where Cartesian tensor notation is employed. Here p denotes the scaled pressure and u_i denotes a scaled velocity component. We use the following boundary conditions: (1) the velocity at the edges of the etched hole is equal to zero; (2) above the etched hole, there is a uniform shear flow which we consider undisturbed at a fixed distance from the hole.

2.2
Boundary-integral equations

In this subsection, we derive the standard boundary-integral equations. A fundamental identity for Stokes equations, analogous to Green's identity, may be written as

$$\frac{\partial}{\partial x_j}\left(u_i\sigma^*_{ij} - u^*_i\sigma_{ij}\right) = 0 \ . \tag{2.4}$$

In this expression, $\mathbf{u}$ and $\mathbf{u}^*$ are any two solutions of (2.1) and (2.2) with associated stress tensors $\boldsymbol{\sigma}$ and $\boldsymbol{\sigma}^*$. This identity is easily verified by direct substitution of (2.3). When the identity is integrated over any bounded volume of fluid with boundary S, the divergence theorem may be applied to yield an integral formula known as the reciprocal theorem

$$\int_S (u_i\sigma^*_{ij}n_j - u^*_i\sigma_{ij}n_j)\mathrm{d}l(\mathbf{y}) = 0 \ , \tag{2.5}$$

where $\mathbf{n}$ is the outward unit normal. This integral relation (2.5) was first written down by Lorentz [18].

To obtain an integral formula we choose $\mathbf{u}^*$ to be the fundamental solution for two-dimensional Stokes flow. This solution was also derived in [18]. We shall use the representation which is given in [11]:

$$u^*_i(\mathbf{y}) = S_{il}(\mathbf{x},\mathbf{y})\frac{q_l(\mathbf{x})}{4\pi} \ , \tag{2.6}$$

where $r = |\mathbf{y} - \mathbf{x}|$ and

$$S_{il}(\mathbf{x},\mathbf{y}) = -\delta_{il}\ln r + \frac{(y_i - x_i)(y_l - x_l)}{r^2} \ . \tag{2.7}$$

Physically, this may be interpreted as the velocity at position $\mathbf{y}$ induced by a two-dimensional point force $\mathbf{q}$ at position $\mathbf{x}$. From (2.6) and (2.1) the pressure can be obtained as:

$$p^*(\mathbf{y}) = 2\frac{y_l - x_l}{r^2}\frac{q_l(\mathbf{x})}{4\pi} \ . \tag{2.8}$$

The stress tensor associated with the velocity (2.6) is given by

$$\sigma^*_{il}(\mathbf{y}) = T_{ikl}(\mathbf{x},\mathbf{y})\frac{q_k(\mathbf{x})}{4\pi} \ , \tag{2.9}$$

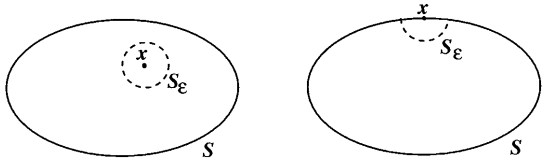

Fig. 4. Definition of S_ϵ for a point inside the domain and on the boundary

where the elements of T_{ikl}, which can be derived from (2.3), are defined by

$$T_{ikl}(\mathbf{x},\mathbf{y}) = -4\frac{(y_i - x_i)(y_k - x_k)(y_l - x_l)}{r^4} \quad . \tag{2.10}$$

When the integral formula (2.5) is applied, with $\mathbf{u}^*$ and $\boldsymbol{\sigma}^*$ given by (1) and (4), the boundary surface includes two components: S which represents all surfaces bounding the domain and S_ϵ, which is a circle or semi-circle (see Fig. 4) with radius ϵ and midpoint $\mathbf{x}$. Evaluating the integral over S_ϵ in the limit as $\epsilon \to 0$, we have

$$u_i(\mathbf{x}) = \frac{1}{4\pi}\int_S [S_{il}(\mathbf{x},\mathbf{y})f_l(\mathbf{y}) - T_{ikl}(\mathbf{x},\mathbf{y})u_k(\mathbf{y})n_l(\mathbf{y})]\mathrm{d}l(\mathbf{y}) \quad , \tag{2.11}$$

when the point $\mathbf{x}$ is in the volume of fluid, and

$$u_i(\mathbf{x}) = \frac{1}{2\pi}\int_S [S_{il}(\mathbf{x},\mathbf{y})f_l(\mathbf{y}) - T_{ikl}(\mathbf{x},\mathbf{y})u_k(\mathbf{y})n_l(\mathbf{y})]\mathrm{d}l(\mathbf{y}) \quad , \tag{2.12}$$

when $\mathbf{x}$ is located on a smooth part of the boundary of the domain. In (2.11) and (2.12), $f_j(\mathbf{y})$ is the surface-force vector defined as $f_j(\mathbf{y}) = \sigma_{jk}(\mathbf{y})n_k(\mathbf{y})$. Because, for this flow problem, the velocity components are known at the boundary, (2.12) is a Fredholm integral equation of the first kind for the unknown $\mathbf{f}$ at the boundary S. With the solution of $\mathbf{f}$ (2.11) can be used to compute $\mathbf{u}$ in an arbitrary point inside the domain.

A disadvantage of numerical methods which solve (2.12) for the unknown $\mathbf{f}$ is that the resulting matrix becomes more and more singular as the number of boundary elements is increased. To avoid this we use a Fredholm integral equation of the second kind instead of (2.12). An equation similar to the Fredholm integral equation of the first kind can be derived for the surface-force vector. To arrive at such an equation we define

$$P(\mathbf{x}) = \frac{1}{2\pi}\int_S [p_l(\mathbf{x},\mathbf{y})f_l(\mathbf{y}) - \Pi_{kl}(\mathbf{x},\mathbf{y})u_k(\mathbf{y})n_l(\mathbf{y})]\mathrm{d}l(\mathbf{y}) \tag{2.13}$$

for a point $\mathbf{x}$ on a smooth part of the boundary of the domain. Here, Π_{kl} is given by:

$$\Pi_{kl}(\mathbf{x},\mathbf{y}) = 2\left(-\frac{\delta_{kl}}{r^2} + 2\frac{(y_k - x_k)(y_l - x_l)}{r^4}\right) \quad . \tag{2.14}$$

By substitution of (2.13) and (2.12) in (2.3) a Fredholm integral equation of the second kind is found for the surface-force vector $\mathbf{f}$ (*i.e.* for a point $\mathbf{x}$ on the boundary) [14]:

$$\begin{aligned} f_i(\mathbf{x}) = {} & \delta_{ij}\left[\frac{1}{2\pi}\int_S (-p_l(\mathbf{x},\mathbf{y})f_l(\mathbf{y}) \right. \\ & \left. + \Pi_{kl}(\mathbf{x},\mathbf{y})u_k(\mathbf{y})n_l(\mathbf{y}))\mathrm{d}l(\mathbf{y})\right]n_j(\mathbf{x}) \\ & + \frac{\partial}{\partial x_j}\left[\frac{1}{2\pi}\int_S (S_{il}(\mathbf{x},\mathbf{y})f_l(\mathbf{y}) \right. \\ & \left. - T_{ikl}(\mathbf{x},\mathbf{y})u_k(\mathbf{y})n_l(\mathbf{y}))\mathrm{d}l(\mathbf{y})\right]n_j(\mathbf{x}) \\ & + \frac{\partial}{\partial x_i}\left[\frac{1}{2\pi}\int_S (S_{jl}(\mathbf{x},\mathbf{y})f_l(\mathbf{y}) \right. \\ & \left. - T_{jkl}(\mathbf{x},\mathbf{y})u_k(\mathbf{y})n_l(\mathbf{y}))\mathrm{d}l(\mathbf{y})\right]n_j(\mathbf{x}) \quad . \end{aligned} \tag{2.15}$$

Equation (2.15) can be rewritten as

$$f_i(\mathbf{x}) = \int_S \left[W_{il}(\mathbf{x},\mathbf{y})f_l(\mathbf{y}) + \pi^*_{ikl}(\mathbf{x},\mathbf{y})u_k(\mathbf{y})n_l(\mathbf{y})\right]\mathrm{d}l(\mathbf{y}) \quad , \tag{2.16}$$

where

$$W_{il} = \frac{1}{2\pi}\left[-\delta_{ij}p_l + \frac{\partial S_{il}}{\partial x_j} + \frac{\partial S_{jl}}{\partial x_i}\right]n_j \quad , \tag{2.17}$$

and

$$\pi^*_{ikl} = \frac{1}{2\pi}\left[\delta_{ij}\Pi_{kl} - \frac{\partial T_{ikl}}{\partial x_j} - \frac{\partial T_{jkl}}{\partial x_i}\right]n_j \quad . \tag{2.18}$$

Using the theory as described by [3] Eq. (2.16) can be transformed to

$$\begin{aligned} f_i(\mathbf{x}) = \int_S & [W_{il}(\mathbf{x},\mathbf{y})f_l(\mathbf{y}) + \pi^*_{ikl}(\mathbf{x},\mathbf{y})(u_k(\mathbf{y}) \\ & - u_k(\mathbf{x}))n_l(\mathbf{y})]\mathrm{d}l(\mathbf{y}) \quad . \end{aligned} \tag{2.19}$$

The singularity in the kernels of (2.19) is removed in a similar way as described in Okada et al. [21], Kaya and Ergodan [15] and Chien et al. [3]. Equation (2.19) will be the basic equation for the computations.

2.3 Boundary-integral expression for the stream function

In this subsection, a new boundary-integral expression for the stream function will be derived to complete the set of equations described in the previous subsection. This derivation starts with the definition of the stream function Ψ:

$$u_1 = \frac{\partial \Psi}{\partial x_2} \quad \text{and} \quad u_2 = -\frac{\partial \Psi}{\partial x_1} \quad . \tag{2.20}$$

We assume that the stream function can be written as a boundary integral of the form

$$\Psi(\mathbf{x}) = \frac{1}{4\pi}\int_S [I_j(\mathbf{x},\mathbf{y})f_j(\mathbf{y}) + H_{jk}(\mathbf{x},\mathbf{y})n_k(\mathbf{y})u_j(\mathbf{y})]\mathrm{d}l(\mathbf{y}) \quad , \tag{2.21}$$

for a point $\mathbf{x}$ inside the fluid domain. When (2.11) and (2.21) are substituted in (2.20), equations can be derived for the unknown kernels $I_j(\mathbf{x},\mathbf{y})$ and $H_{jk}(\mathbf{x},\mathbf{y})$:

$$\frac{\partial I_j}{\partial x_1} = -S_{2j} \quad \frac{\partial H_{jk}}{\partial x_1} = T_{2jk}$$
$$\frac{\partial I_j}{\partial x_2} = S_{1j} \quad \frac{\partial H_{jk}}{\partial x_2} = -T_{1jk} \quad .$$

A solution is given by

$$I_1(\mathbf{x},\mathbf{y}) = (y_2 - x_2)\ln r - (y_2 - x_2) \quad ,$$
$$I_2(\mathbf{x},\mathbf{y}) = -(y_1 - x_1)\ln r + (y_1 - x_1) \quad ,$$

and

$$H_{11}(\mathbf{x},\mathbf{y}) = -2\frac{(y_1 - x_1)(y_2 - x_2)}{r^2} - 2\ \arctan\ \frac{y_2 - x_2}{y_1 - x_1} \quad ,$$
$$H_{12}(\mathbf{x},\mathbf{y}) = H_{21}(\mathbf{x},\mathbf{y}) = \frac{(y_1 - x_1)^2 - (y_2 - x_2)^2}{r^2} \quad ,$$
$$H_{22}(\mathbf{x},\mathbf{y}) = \frac{(y_1 - x_1)(y_2 - x_2)}{r^2} - 2\ \arctan\ \frac{y_2 - x_2}{y_1 - x_1} \quad .$$

This expression is only valid if the arctan function is treated in a special way. In the formulation for the stream function the path over which is integrated encircles the point (x_1, x_2). On this path the arctan function has two jumps at $y_1 = x_1$: One for a positive and one for a negative value of $y_2 - x_2$. One jump can be removed by addition of a constant to the values with $y_2 - x_2$ larger than zero. By addition or subtraction of a constant, the position of the second jump is placed at a fixed boundary point. In this way, we can compute the stream-function value in every interior point.

Together with this boundary-integral formulation, we have a complete set of expressions for the stream function and the velocity and shear-stress components.

2.4
Singularity subtraction

In the geometry as depicted in Fig. 1 there are sharp corners. For the second derivatives of the stream function singularities arise at these corners. This problem was encountered by Moffatt [20] and later discussed for several examples by Lugt [19]. In both papers, expressions are derived for the singular behavior. To regularize the integrals near the corners, this behavior can be included in the integral equations. This singularity-subtraction method was used in [2, 10, 16] to increase the accuracy of the computations. In this subsection the application of this method to the etch-hole geometry is described.

In [19] solutions for the biharmonic equation around a corner in plane polar coordinates (r,θ) are determined:

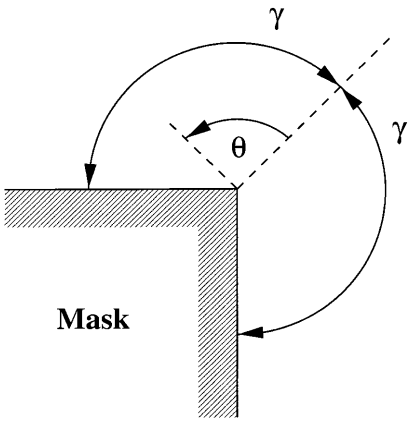

Fig. 5. Definition of γ and θ

$$\Psi = r^{\lambda+1}[A\cos(\lambda+1)\theta + B\sin(\lambda+1)\theta + C\cos(\lambda-1)\theta + D\sin(\lambda-1)\theta], \quad \lambda \neq 1 \quad , \tag{2.22}$$

and

$$\Psi = r^2[A\cos 2\theta + B\sin 2\theta + C\theta + D], \quad \lambda = 1 \quad , \tag{2.23}$$

where r is the distance to the corner, λ may be called the exponent of the solution and θ is the angle as shown in Fig. 5. In the boundary-element computations, second derivatives of the stream function are used. These quantities are singular if $\lambda < 1$. Solutions with $Re(\lambda) < 0$ are physically irrelevant. The boundary conditions at a mask-edge corner are

$$\Psi = 0 \quad \text{and} \quad \frac{\partial \Psi}{\partial \theta} = 0 \quad \text{at } \theta = -\gamma \quad \text{and} \quad \theta = \gamma \quad ,$$

where 2γ is the mask-edge corner, which will normally vary between π and 2π. To obtain equations for the singular exponents λ, (2.22) is divided into so-called symmetric solutions with A and C equal to zero, and skew-symmetric solutions with B and D equal to zero [19]. When the boundary conditions are substituted in the symmetric solutions the equation for λ becomes

$$\sin 2\gamma\lambda = \lambda \sin 2\gamma \quad , \tag{2.24}$$

and for the skew-symmetric solutions this equation is

$$\sin 2\gamma\lambda = -\lambda \sin 2\gamma \quad , \tag{2.25}$$

The value $\lambda = 1$ is a special case. It can be derived from (2.23) together with the boundary conditions that this solution of λ can only be found for corners $2\gamma_1$ with

$$\tan 2\gamma_1 = 2\gamma_1 \tag{2.26}$$

in the symmetric case and

$$\tan 2\gamma_1 = 0 \tag{2.27}$$

in the skew-symmetric case. For the symmetric case $2\gamma_1$ is approximately equal to 1.4303π. For different corners 2γ the first solutions of λ_a in the skew-symmetric case, and λ_s in the symmetric case, are given in Table 1. There is one singular solution for corners $2\gamma \leq 2\gamma_1$ and there are two singular solutions for corners $2\gamma_1 \leq 2\gamma \leq 2\pi$. For a corner

Table 1. First two values of λ for a number of angles

2γ	$7\pi/6$	$8\pi/6$	$2\gamma_1$	$9\pi/6$	$10\pi/6$	$11\pi/6$	2π
λ_a	0.75197	0.61573	0.56829	0.54448	0.51222	0.50145	0.50000
λ_s	1.48581	1.14891	1.00000	0.90853	0.73090	0.59819	0.50000

2π, which corresponds to an infinitely thin mask, there is one double solution. For every singular λ, an eigenfunction can be derived with an unknown coefficient. In our application 2γ is equal to $3\pi/2$ and we include the two corresponding singular solutions in the integral formulations. The solutions at the corners satisfy the Stokes equations, so we can subtract the integral equations for these solutions from the integral equations [16, 10]. This results for example for the shear-stress component f_i in case of two singular exponents in

$$f_i^r = f_i - A_a f_i^{s_1} - A_s f_i^{s_2} \quad , \tag{2.28}$$

where $f_i^{s_1}$ is the behavior near the corner which results from λ_a, and $f_i^{s_2}$ is the behavior near the corner which results from λ_s. In the boundary-element computations we start with the equation for the resulting shear-stress components f_i^r, which are regular near the corners. In further computations we will denote them also as the regular quantities. The introduction of the two coefficients A_a and A_s in (2.28) necessitates the use of two additional equations. These are extracted from the assumption that the shear stress near a corner is completely determined by the singular behavior. When we consider a geometry with only one sharp corner, the extra equation

$$0 = f_i - A_a f_i^{s_1} - A_s f_i^{s_2} \tag{2.29}$$

is obtained. This equation is applied to the component f_i which does not include the pressure.

The shear stress has one component in which the pressure appears. From the Stokes equations it is clear that we may add a constant to the pressure without changing the values of the velocities. In the first step in this iterative solution scheme, which will be described in the next subsection, velocities are prescribed at the boundaries, but the shear stress is not prescribed anywhere. To obtain a unique solution for these shear-stress components, we have to prescribe the pressure at a certain point. For the analytical description of the stream function near the mask-edge corners, the same theory holds. An expression for the pressure can be determined up to a constant. This is the reason for prescribing the equations for the unknown coefficients near the corner only for that part of the shear stress which does not include the pressure.

In the numerical computations, there is no collocation point at the corner. The value for the regular shear stress at the corner is extrapolated from the three nearest points. This is done from both sides of the corners, which results in two equations for the two unknown coefficients. In this way, the system is solved for the regular quantities. Afterwards, the values of the quantities we want to know are computed by addition of the singular parts of the solution. Only corners $2\gamma = 3\pi/2$ are encountered in the computations presented, but it is clear that the method is applicable to other corners.

2.5 Domain decomposition

The last step needed for the computations is a description of the domain decomposition. In the previous subsections equations for the boundary-element method including the singular behavior are described. The singular behavior is subtracted from the equations, and afterwards added to the regular parts of the solution. However, this approach has a disadvantage. In parts of the domain where the velocity is very small, e.g. near the bottom of the etch hole, the regular and singular parts of the solution are of almost equal magnitude, but different sign. Hence, small relative errors in the two contributions may result in large relative errors in the velocity components. This behavior can be avoided by domain decomposition. We divide the etch-hole geometry in two sub-domains as depicted in Fig. 3. We compute solutions for the fluid flow in both sub-domains. An advantage of this computation is that in sub-domain II we do not have to take into account the behavior of the fluid flow near the corners in sub-domain I. At the interface of these sub-domains the shear-stress as well as the velocity components are unknown. We have to compute these quantities with an iterative procedure. In this paper, we first choose initial values for the velocity components. We compute an approximation for the shear-stress components with the equations for the first sub-domain. These stress components are used in the second domain to compute a new approximation for the velocity components, and so on. This so-called Neumann–Dirichlet preconditioning [4, 8, 9, 12] is used to compute the unknown quantities:

- In sub-domain I new approximations of the shear stresses at the domain interface are computed. In these computations, integral equation (2.19) is used for the shear-stress components. With these new approximations of the shear stresses, new boundary conditions for the second sub-domain are computed by

$$f_i^{\text{new}} = \alpha f_i^{\text{old}} + (1-\alpha) f_i^{\text{new}} \quad . \tag{2.30}$$

- In sub-domain II new approximations of the velocity components at the domain interface are computed. In these computations, integral equation (2.12) is used for the interface, while (2.19) is used for the unknown shear stresses at the boundaries of this sub-domain. With these new approximations, new boundary conditions for the first sub-domain are computed at the domain interface by

$$u_i^{\text{new}} = \alpha u_i^{\text{old}} + (1-\alpha) u_i^{\text{new}} \quad . \tag{2.31}$$

This algorithm is repeated until the old and new velocity and shear-stress components have converged. In the next section, different values of α are compared and it is shown that the convergence is independent of the number of boundary elements and of the shape of the etch hole.

This domain decomposition has a second advantage: to compute a numerical simulation of wet-chemical etching, the flow needs to be computed in each time step for a geometry in which the etch-hole grows. However, during the etch process the geometry of the first sub-domain of Fig. 3 remains the same. With domain decomposition it is

not necessary to recompute the matrix for the unknown quantities of this sub-domain which saves much CPU-time.

Instead of using two sub-domains one could think of an algorithm with a sub-domain around each singular corner. This would have the disadvantage that the iterative process becomes much more complicated. With the two sub-domain algorithm as described in this section, the largest order differences of the singular quantities are separated. The accuracy of the results obtained with this algorithm shows that it is not necessary to increase the number of sub-domains.

3
Numerical implementation and validation

In Sect. 2 we derived the equations used to compute the stream function and the velocity and shear-stress components. In this section the numerical implementation is described and validated.

To obtain a numerical solution the continuous boundary is represented by a number of discrete boundary elements and **u** and **f** on the boundary are expressed in terms of their values at a number of discrete boundary points. The elements are chosen in such a way that the corners lay at the end of a line segment. Equation (2.19) combined with the discretized boundary conditions, leads to a system of linear algebraic equations for the unknown shear-stress **f** at the discrete boundary points. For the second sub-domain we discretize (2.12) for the domain-decomposition boundary. These linear systems are solved using Gaussian elimination.

Quadratic polynomials are used to describe the shape of the boundary elements. For the approximation of unknown quantities **f** or **u** at the boundary quadratic polynomials are used too. The numerical integration for the regular integrals is evaluated by using standard Gaussian Quadrature.

In this section we first show the improvement of the accuracy of the computed solution when singularity subtraction is used. We apply this subtraction to a geometry without domain decomposition.

As the authors could not find an earlier application of domain decomposition in Stokes flow, it is shown in the second subsection that the iterative algorithm, as it is described in the previous section, converges to the known solution for a standard problem. We show some convergence results for different values of the iteration parameter α, for different grid sizes and for different shapes of the etch hole.

Domain decomposition improves the accuracy of the solution in the etch-hole approximation. This is shown in the third subsection.

In the last subsection the accuracy is verified by comparison with the semi-analytical results from [6].

3.1
Improved accuracy with singularity subtraction

In this subsection we will show that singularity subtraction improves the accuracy of the results. A rectangular geometry of a cavity is considered, which can be described by Fig. 6.

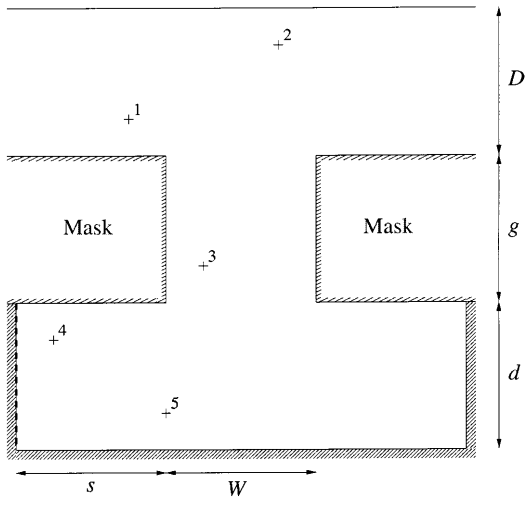

Fig. 6. Geometry used for validation at dashed line and at the interior points

In [6] the velocity component in 5 interior points was presented (see Fig. 6 for locations). These results are very accurate, and will be used as a benchmark for the boundary-element method.

In the first group of results of Table 2 the velocity components are computed with a standard boundary-element method (BEM I) with an equidistant grid distribution for different numbers of elements. In Table 2 also the values of the velocity components as computed in [6] are given. By comparison it is easy to see that the boundary-element computations are inaccurate, especially in points inside the hole. In this geometry, four sharp corners are present to which singularity subtraction can be applied. The second group of results is computed with a boundary-element method with a standard grid and singularity subtraction (BEM II), as described in Sect. 2.4. We see that singularity subtraction improves the results considerably.

Another possibility to improve the results is grid refinement. We have made a new grid in which the boundary-element size is a quadratic function of the distance r to the corner. The idea is that the fluid flow is dominated by the singularities at the corners. By putting more elements near these corners, we hope to get better results. The results of this boundary-element computation (BEM III) is given in the third group of results. With respect to the first situation the results are better, but the singularity subtraction still gives the much better results at locations where the velocity is small.

One could think of the possibility of moving more collocation points towards the corner. The disadvantage is that the number of boundary elements further away from the corner would become very low, which will affect the accuracy in these regions.

In the last group of results the algorithm uses a refined grid near the corners as well as singularity subtraction (BEM IV). The results are of a similar order of accuracy as the results with a normal grid. This could be expected because the singularity subtraction avoids the singular behavior near the corners and thus the need for grid refinement.

Table 2. Velocity components at given points as a function of the number of boundary elements (N) computed with a normal boundary-element method (I), with singularity subtraction (II), with grid refinement (III), with singularity subtraction and grid refinement (IV) and computed with the method of series expansions [6]

		Point 1	Point 2	Point 3	Point 4	Point 5
	x	−1.5	0.5	−0.5	−2.5	−1.0
	y	0.5	1.5	−1.5	−2.5	−3.5
BEM	N	u (10^{-1} m s^{-1})	v (10^{-3} m s^{-1})	v (10^{-3} m s^{-1})	u (10^{-6} m s^{-1})	v (10^{-5} m s^{-1})
	640	2.53959	4.1555	2.0906	−571.27	−38.269
	960	2.53941	4.1197	2.3998	−430.72	−35.947
I	1280	2.53957	4.0945	2.6219	−353.78	−33.754
	1920	2.54006	4.0606	2.9262	−269.45	−30.285
	2560	2.54051	4.0381	3.1304	−222.93	−27.735
	640	2.54643	3.8567	4.8507	−6.6162	−2.4186
	960	2.54644	3.8550	4.8604	−6.0597	−2.2365
II	1280	2.54644	3.8544	4.8639	−5.8588	−2.1708
	1920	2.54644	3.8539	4.8665	−5.7105	−2.1230
	2560	2.54644	3.8537	4.8674	−5.6569	−2.1063
	640	2.54612	3.8747	4.6828	−37.676	−4.6597
	960	2.54622	3.8654	4.7619	−22.219	−3.6024
III	1280	2.54627	3.8613	4.7974	−16.162	−3.1097
	1920	2.54633	3.8578	4.8284	−11.264	−2.6689
	2560	2.54636	3.8563	4.8419	−9.2736	−2.4760
	640	2.54659	3.8518	4.8911	−5.0576	−1.7632
	960	2.54650	3.8528	4.8769	−5.4097	−1.9712
IV	1280	2.54647	3.8531	4.8728	−5.5013	−2.0290
	1920	2.54645	3.8533	4.8702	−5.5544	−2.0640
	2560	2.54644	3.8534	4.8694	−5.5570	−2.0747
[6]		2.54631	3.8543	4.8685	−5.5879	−2.0775

We can conclude from Table 2 that singularity subtraction is a useful tool to increase the accuracy of the computations. A similar conclusion was stated in Floryan and Czechowski [7] for the singularity subtraction using a streamfunction-vorticity formulation.

3.2
Convergence of the domain-decomposition algorithm

Since we were unable to find an earlier application of the domain-decomposition technique to Stokes flow, we will show the convergence of the iterative procedure as described in the previous section for a standard problem.

The Stokes equations are solved by the domain-decomposition algorithm for an etch-hole geometry as depicted in Fig. 6 with all geometric parameters equal to unity. The boundary conditions are modified. We assume a linear velocity profile $u_1 = y/2$ for all boundary points. Thus, the solution is known beforehand, and we can check whether the iterative procedure converges to this solution. The extra boundary which is the interface between the sub-domains is chosen at the same position as in the etch problem: in the middle of the mask-edges.

In the scheme described in subsection 2.5 the algorithm stops if the approximations of the velocity and shear-stress components computed on the interface in the sub-domains have converged. We measure this convergence by computing the l_2-norm for the differences of the quantities from the sub-domains.

In the scheme a parameter α is used to compute new approximations of the velocity and shear-stress components. In Fig. 7 the convergence of the procedure is shown for several values of α. The l_2-norm of the differences of the velocity components u_i^{old} and u_i^{new}, as described in (2.31), is shown as a function of the iteration number k. From this figure we infer that a value of α around 0.5 works well. In the remainder of this paper we choose $\alpha = 0.5$.

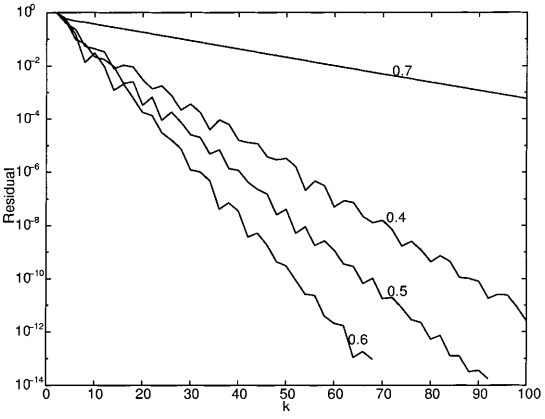

Fig. 7. Convergence behavior of the domain-decomposition method for several values of α

3.3
Improved accuracy with domain decomposition

In the previous section the domain-decomposition technique is described. With the iterative scheme the unknown

quantities are computed for both sub-domains. We will show in this subsection that domain decomposition improves the accuracy. In Table 2 the results for a normal grid without domain decomposition are given in the first group of results computed with a normal boundary element method (BEM I). In Table 3 the results for a normal grid with domain decomposition are given in the first group of results (BEM V). From these results we can conclude that for a normal grid without singularity subtraction, domain decomposition improves the results significantly. Another possibility to avoid domain decomposition could be a grid refinement near the singular corners, which was already shown in Table 2 with BEM III. The upper points are more accurate with grid refinement (BEM III) because with grid refinement the singular behavior at the corners is approximated better. The lower points are more accurate with domain decomposition (BEM V).

The best results can be obtained when grid refinement as well as domain decomposition are used (BEM VI). These results are shown in the second group of results of Table 3.

For these computations, singularity subtraction can be applied too. As mentioned in the previous subsection, when singularity subtraction is used it does not make much difference whether we use a refined grid or not. The third group of results in Table 3 is the boundary-element method with a normal grid, using domain decomposition and singularity subtraction (BEM VII). The last group of results is a similar boundary-element method with a refined grid (BEM VIII). The method with a refined grid seems to be slightly more accurate for the computations with a low number of grid points.

One may wonder whether it is really necessary to use a domain decomposition when singularity subtraction is applied. Comparing BEM IV and BEM VIII with the semi-analytical results from [6], it is difficult to see from these five points which method is more accurate. We have to look at this in more detail.

First we can consider the differences between the computed velocity components and the semi-analytical results in some extra points. In Table 4 the differences are given for some points at the line $y = -3.5$. The method with domain decomposition as well as singularity subtraction (BEM VII) is the most accurate. We can see that the method with grid refinement near the singular corners is less accurate in regions far away from the corners than the method without grid refinement. This can be explained by the fact that, as a result of the refinement near the corners, there are less points further away.

Another comparison can be made for the shear stress. We compute the second shear-stress component f_2 at the dashed line at the left-hand side along the etch-hole boundary (see Fig. 6). In Fig. 8 the results are plotted for computations with BEM VII (solid line), BEM II (dashed line) and the semi-analytical solution. The computation without domain decomposition shows large deviations from the semi-analytical solution. In contrast, the results of the system with domain decomposition agree very well with the semi-analytical solution. From the presented tables and figures is it clear that the results are improved by the use of domain decomposition.

Table 4. Differences of velocity in y-direction (10^{-7} m s^{-1}) at points with $y = -3.5$ computed with the finest grid and the results from [6]

x	−2.5	−2.0	−1.5	−1.0	−0.5
BEM II	1.78	2.49	2.47	2.82	0.74
BEM IV	2.28	2.52	2.19	0.34	0.60
BEM VII	0.05	0.13	0.14	0.84	0.58
BEM VIII	1.18	1.56	1.46	1.72	0.01

Table 3. Velocity components at given points as a function of the number of boundary elements (N) computed with a boundary-element method with domain decomposition (V), with domain decomposition and grid refinement (VI), with domain decomposition and singularity subtraction (VII) and with domain decomposition, singularity subtraction and grid refinement (VIII) and computed with the method of series expansions [6]

BEM	N	Point 1 u (10^{-1} m s^{-1})	Point 2 v (10^{-3} m s^{-1})	Point 3 v (10^{-3} m s^{-1})	Point 4 u (10^{-6} m s^{-1})	Point 5 v (10^{-5} m s^{-1})
	640	2.55167	3.9914	4.7456	−8.7123	−1.2129
	960	2.55035	3.9709	4.7602	−7.3280	−1.4188
V	1280	2.54964	3.9575	4.7705	−6.7431	−1.5308
	1920	2.54886	3.9406	4.7844	−6.2392	−1.6542
	2560	2.54843	3.9299	4.7936	−6.0224	−1.7232
	640	2.54663	3.8670	4.8967	−5.7958	−2.1466
	960	2.54648	3.8612	4.8892	−5.5679	−2.1148
VI	1280	2.54644	3.8588	4.8849	−5.5526	−2.1020
	1920	2.54641	3.8566	4.8801	−5.5662	−2.0928
	2560	2.54641	3.8556	4.8774	−5.5762	−2.0897
	640	2.54621	3.8599	4.9069	−6.1757	−2.0740
	960	2.54627	3.8573	4.8949	−5.8535	−2.0810
VII	1280	2.54631	3.8561	4.8886	−5.7432	−2.0834
	1920	2.54635	3.8551	4.8821	−5.6633	−2.0852
	2560	2.54637	3.8546	4.8787	−5.6341	−2.0859
	640	2.54617	3.8576	4.9058	−5.4716	−2.1851
	960	2.54626	3.8562	4.8942	−5.5544	−2.1356
VIII	1280	2.54630	3.8555	4.8882	−5.5023	−2.1156
	1920	2.54634	3.8548	4.8819	−5.5460	−2.1002
	2560	2.54636	3.8544	4.8786	−5.5655	−2.0946
[6]		2.54631	3.8543	4.8685	−5.5879	−2.0775

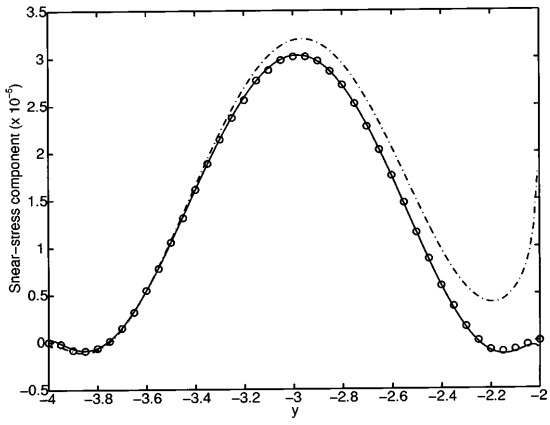

Fig. 8. Boundary-element method results without (dashed line) and with (solid line) domain decomposition and the results of the method of series expansions (circles)

3.4 Accuracy

From the computed quantities in Tables 2 and 3 it can be inferred that the overall convergence of the computed results is linear as a function of the element size. Some of the quantities seem to converge quadratically which can be explained by the following theory.

In general, the computed values can be written as a function of the number of boundary-elements N as

$$V_{ij}^{(N)} = V_{ij}^{(\infty)} + \gamma/N + \zeta/N^2 + o(1/N^2) \ . \qquad (3.32)$$

By application of Richardson extrapolation the values of γ and ζ can be computed. In some cases, γ is so small that γ/N is small compared to ζ/N^2. In these cases, it looks like quadratic convergence. The same convergence behavior can be seen for the singular coefficients. In the computations for the rectangular geometry four singular corners are present. For each corner, the first two singular values λ_1 and λ_2, as computed in Sect. 2, are included in the computations. Hence, there are four pairs of coefficients A_1, A_2 as mentioned in (2.28). Because of the symmetry of the flow problem, the coefficients of the corners at the left mask-edge in Fig. 6 are directly related to the coefficients of the corners at the right mask-edge. Therefore, we only present the values of the first two pairs of coefficients. The coefficients at the upper corner are called A_{11} and A_{12} and the coefficients at the lower corner are called A_{21} and A_{22}. In Table 5 the values are given as a function of the number of boundary elements (N), computed with BEM VII. It is clear that the convergence of the coefficients A_{11} and A_{12} is linear. In contrast, it appears that A_{21} converges quadratically. This can be explained by the argument above.

Table 5. Values of singular coefficients as a function of the number of elements N

N	$A_{11}(10^{-1})$	$A_{12}(10^{-1})$	$A_{21}(10^{-4})$	$A_{22}(10^{-3})$
640	−3.73359	8.96975	8.37946	−8.20534
960	−3.74407	8.96856	7.86911	−8.20352
1280	−3.74994	8.96799	7.76675	−8.20154
1920	−3.75637	8.96748	7.75148	−8.19807
2560	−3.75985	8.96725	7.74624	−8.19550

The coefficient A_{22} converges very slowly, but the differences in the values of this coefficient as N increases are small. We can conclude that this value is already accurately computed for the larger boundary-element sizes.

In Table 6 the values of $\mathbf{u}^{(\infty)}$, computed with the three finest boundary-element sizes from the boundary element computations (BEM VII), are shown along with the corresponding results from [6]. When we compare the values from the method of series expansions with the results of the boundary-element method small differences are noticed. Although the differences are small, especially in the first 4 points, they can be explained in the following way.

The most important reason for these differences is the difference in boundary conditions for both methods. In the boundary-element computations we assume that the uniform shear flow is undisturbed at a fixed distance from the hole. However, in the method of series expansions, we assume that the flow reaches an undisturbed profile at infinity. To check whether this may be a reason for the differences, the velocity components were computed again with the boundary-element method, but now with new boundary conditions: With the method of series expansions, the velocity components at the mentioned fixed distance from the hole are computed and used as boundary conditions for the boundary-element method. This computation is repeated for every boundary-element size. In Table 5 the values of $\mathbf{u}^{(\infty)}$ (BEMB), computed by extrapolation of the three finest boundary-element sizes, are shown along with the corresponding results from [6] and the boundary-element results from the method with the undisturbed boundary conditions (BEM). It is clear that for points 1 and 2 the results are improved by the new boundary conditions. From points 3–5 it can be inferred that the results between and under the masks do not change significantly.

Another reason for the differences in the results is the numerical truncation error. A part of this error is removed by extrapolation, but when this extrapolation is repeated for different boundary-element sizes, the results are different too. It can be concluded that the results still change as the boundary-element size decreases.

Table 6. Extrapolated velocity components from the boundary-element method (BEM VII), the boundary-element method with modified boundary conditions (BEMB) and the values computed in [6]

	Point 1 u (10^{-1} m s^{-1})	Point 2 v (10^{-3} m s^{-1})	Point 3 v (10^{-3} m s^{-1})	Point 4 u (10^{-6} m s^{-1})	Point 5 v (10^{-5} m s^{-1})
BEM	2.54643	3.85334	4.86850	−5.58919	−2.08705
BEMB	2.54630	3.85409	4.86856	−5.58888	−2.08677
[6]	2.54631	3.85434	4.86846	−5.58793	−2.07749

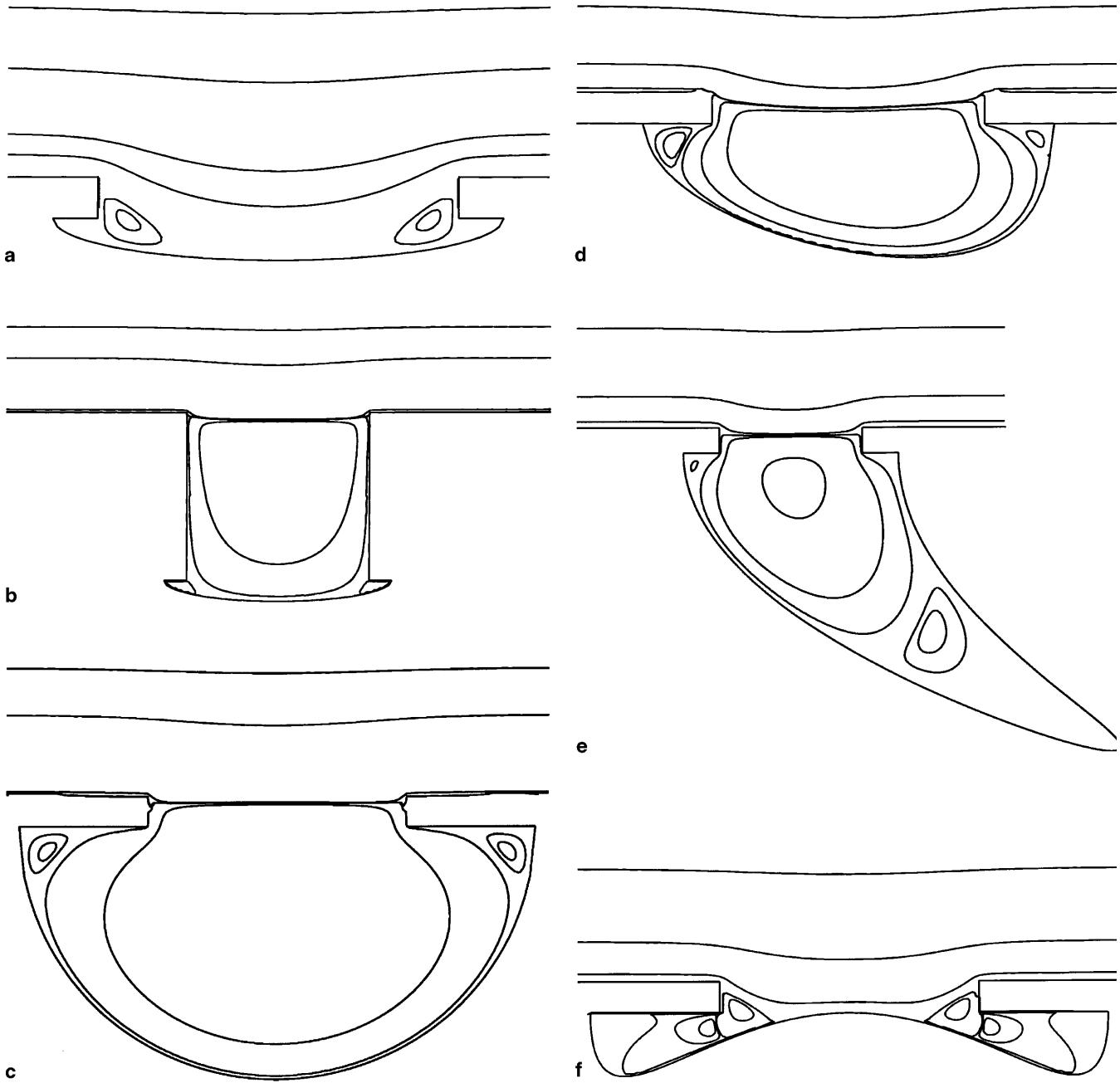

Fig. 9a-f. Iso lines of the stream function for various etch-hole geometries

When we study the differences between the extrapolated boundary-element results and the extrapolated results of the method of series expansions, the largest relative error can be found in point 5. There is a reason for this error which was already mentioned in [6]: In the method of series expansions, the domain is subdivided in seven rectangular sub-domains. In each of these sub-domains, the solution is prescribed by a series expansion. These series converge fast for the interior points of these regions, which gives convergence results which are much more accurate than the boundary-element results. However, the series converge slowly for the points at the interfaces of these regions. Point 5 lies exactly on such an interface, so the result of the method of series expansions is less accurate in this point.

For the etching process, the differences in the results above the etch hole are not so important. Therefore, the boundary-element method without modified boundary conditions is good enough to use in the etch simulation. When we look at the errors between the methods, we see that the difference between the finest extrapolated result in point 3 from BEM and the result from the method of series expansions is very small. The relative difference in point 4 is about 0.02%. This difference is not that big either, and taking into account that the absolute difference is in the order of $10^{-9}\,\mathrm{ms}^{-1}$, we can conclude that the agreement

between the results of both methods confirms the quality of the boundary-element method.

In a numerical simulation of wet-chemical etching, the boundary-element method will be used each time step to compute the fluid flow. In such an application, with a boundary-element size of approximately $h = 1/40$, one computation for the fluid flow takes approximately 1 min on a single R10000 processor.

4 Results and conclusions

With the domain-decomposition method including the singularity-subtraction as described in Sect. 2 the shear-stress and velocity components are computed at the boundary and at the domain-decomposition interface. Afterwards the stream function is computed with the new integral formulation as described in Subsection 2.4.

The number of boundary elements is chosen in such a way that all elements have about the same size, which is equal to $h = 1/N \approx 1/80$. In this section we show the results of the algorithm for different kinds of etch-hole geometries. The first configuration we present in Fig. 9a can be related to a situation in which etching has just started. There is not yet a central vortex in the middle of the cavity. On both sides near the masks, small vortices arise, which gives a result which is rather similar to the results of [11]. In such a situation, etching will proceed very fast in the center of the cavity because the dissolved metal is directly transported away.

In Fig. 9b it is shown that a thick mask decelerates the etching process. When the mask is thick in comparison to the width of the etch pattern, a vortex arises between the mask edges.

During the etching process, stream-function patterns such as shown in Fig. 9c or Fig. 9d will arise. Fig. 9c shows a symmetric pattern, while Fig. 9d gives an antisymmetric profile. The last one is more realistic, since the fluid near the bottom of the central vortex is flowing from right to left. Soon after the fluid has reached the etch-hole bottom, it will be more and more saturated with dissolved material, which will result in a decrease in etch-speed along the bottom of the etch-hole.

The last two stream-function figures show some possibilities of the algorithm. In Fig. 9e the antisymmetric geometry is very extreme. In practice, such a situation will not occur. Near the lowest point of the etch hole, no fluid flow can be detected, so etching will proceed very slowly near this point. Fig. 9f shows the vortices arising in a geometry with an extreme undercut effect.

The domain-decomposition algorithm as presented in this paper is very robust for the shown geometries. In Fig. 10 the l_2-norm of the differences of the velocity components at subsequent iterations is shown as a function of the iteration number from the computations for Fig. 9f. The convergence behavior for the other geometries presented is similar. The number of boundary elements does not make a difference in convergence either. We can conclude that the domain-decomposition algorithm is hardly dependent on the shape of the grid or the number of elements.

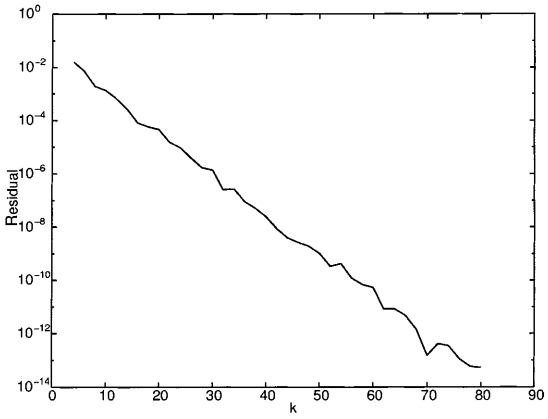

Fig. 10. Convergence of the domain-decomposition algorithm

As mentioned in the introduction, in [17] it is described how to compute the concentration in an etch-hole geometry without overhanging masks from the velocity and shear-stress components. The shear-stress components are needed at the boundary of the cavity, and the velocity components are needed at the separating streamlines. In Fig. 11 the normal stress is depicted along the boundary of the cavity shown in Fig. 9d for different boundary-element sizes. It is clear that already for a small number of boundary elements the results are rather accurate.

Summarizing, we have described an accurate boundary-element method for the computation of Stokes flow in complex geometries. We have shown that the domain-decomposition method converges properly for all flow cases considered. The accuracy of the results is increased by using domain decomposition as well as singularity subtraction. A new integral formulation for the stream function is developed, which makes it very easy to compute dividing streamlines. The method used can be applied to all sorts of etch-hole geometries. The results are verified by comparison with semi-analytical computations for a rectangular etch-hole approximation. The similarity between both results confirms that the described method is very accurate.

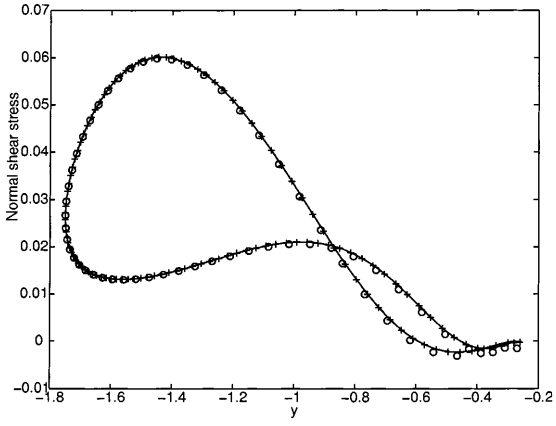

Fig. 11. Normal stress along the boundary of the cavity for $h = 1/20$ (circles), $h = 1/40$ (crosses) and $h = 1/80$ (solid line). The geometry is the same as in Fig. 9d

For the construction of an etch simulation, a model can be developed which uses the boundary-element method results to compute the concentration of dissolved material. This model is described in [5].

The presented boundary-element method can be extended to three-dimensional situations too. Examples are given in [22, 23]. It is easy to extend the domain-decomposition method to three-dimensional geometries [4]. A description of the singular behavior near a sharp corner in three-dimensional formulations can be derived in some special cases. For straight grooves and for axisymmetric holes analytical descriptions of the singular behavior near the sharp rims can be found. These formulations will be published in the near future.

References

1. **Bézine G, Bonneau D** (1981) Integral equation method for the study of two dimensional Stokes flow. Acta Mechanica 41: 197–209
2. **Bohou X** (1985) Some problems in slow viscous flow. Technical report, The Danish Center for Applied Mathematics and Mechanics
3. **Chien CC, Rajiyah H, Atluri SN** (1991) on the evaluation of hyper-singular intergrals arising in the boundary-element method for linear elasticity. Comp. Mech. 8: 57–70
4. **De Haas PCA** (1997) Numerical simulation of nonlinear water waves using a panel method; domain decomposition and applications. PhD thesis, University of Twente, Enschede
5. **Driesen CH, Kuerten JGM, Kuiken HK** (1998) Mass transport in a partially covered fluid-filled cavity. Accepted for publication in Int. J. Heat Mass Transfer, also available as Memorandum No. 1474, University of Twente, The Netherlands
6. **Driesen CH, Kuerten JGM, Streng M** (1998) Low-Reynolds-number flow over partially covered cavities. J. Eng. Math., 34: 5–20
7. **Floryan JM, Czechowski L** (1995) On the numerical treatment of corner singularity in the vorticity field. J. Comp. Phys. 118: 222–228
8. **Funaro D, Quarteroni A, Zanolli P** (1988) An iterative procedure with interface relaxation for domain decomposition methods. SIAM J. Numer. Anal. 25: 1213–1236
9. **Greenbaum A, Greengard L** (1993) Laplace's equation and the Dirichlet-Neumann map in multiply connected domains. J. Comp. Phys. 105: 267–278
10. **Hansen EB, Kelmanson MA** (1994) An integral equation justification of the boundary conditions of the driven-cavity problem. Comp. Fluids 23: 225–240
11. **Higdon JJL** (1985) Stokes flow in arbitrary two-dimensional domains: shear flow over ridges and cavities. J. Fluid Mech. 159: 195–226
12. **Hribersek M, Skerget L** (1996) Domain decomposition methods for fluid flow problems by the boundary domain integral method. Z. Angew. Math. Mech. 76: 425–426
13. **Hsiao GC, Wendland WL** (1991) Domain decomposition in boundary element methods. In: Glowinski R, et al. (ed) Proc. 4th Int. Symp. Domain Decomposition Methods for Partial Differential Equations, p. 41–49, Philadelphia, SIAM
14. **Ingber MS, Mondy LA** (1993) Direct second kind boundary-element integral formulation for Stokes flow problems. Comp. Mech. 11: 11–27
15. **Kaya AC, Ergodan F** (1987) On the solution of integral equations with strongly singular kernels. Q. Appl. Math. 45: 105–122
16. **Kelmanson MA** (1983) Modified integral equation solution of viscous flows near sharp corners. Comp. Fluids 11: 307–324
17. **Kuiken HK** (1978) Heat or mass transfer from an open cavity. J. Eng. Math. 40: 129–155
18. **Lorentz HA** (1896) Eene algemeene stelling omtrent de beweging eener vloeistof met wrijving en eenige daaruit afgeleide gevolgen. Versl. K. Akad. Wetensch. Amsterdam, pages 168–175
19. **Lugt HJ, Schwiderski EW** (1965) Flows around dihedral angles. Proc. R. Soc. Lond. A 285: 382–399
20. **Moffatt HK** (1964) Viscous and resistive eddies near a sharp corner. J. Fluid. Mech. 18: 1–18
21. **Okada H, Rajiyah H, Atluri SN** (1988) A novel displacement gradient boundary-element method for elastic stress analysis with high accuracy. ASME J. Appl. Mech. 55: 786–794
22. **Pozrikidis C** (1994) Shear flow over a plane wall with an axisymmetric cavity or a circular orifice of finite thickness. Phys. Fluids 6: 68–79
23. **Pozrikidis C** (1997) Shear flow over a protuberance on a plane wall. J. Eng. Math. 31: 29–42
24. **Shin CB, Economou DJ** (1989) Effect of transport and reaction on the shape evolution of cavities during wet chemical etching. J. Elchem. Soc. 136: 1997–2004
25. **Shin CB, Economou DJ** (1990) Mass transfer by natural and forced convection in open cavities. Int. J. Heat Mass Transfer 33: 2191–2205